European Journal of Cell Biology 100 (2021) 151180

Contents lists available at ScienceDirect

European Journal of Cell Biology

journal homepage: www.elsevier.com/locate/ejcb

Specific subdomain localization of ER resident proteins and membrane contact sites resolved by electron microscopy

Behnam Lak [a], Shiqian Li [b,c], Ilya Belevich [d], Sreesha Sree [a], Rebeka Butkovic [a], Elina Ikonen [b,c], Eija Jokitalo [a,d,*]

[a] Institute of Biotechnology, Helsinki Institute of Life Science, University of Helsinki, Viikinkaari 9c, 00014 Helsinki, Finland
[b] Department of Anatomy and Stem Cells and Metabolism Research Program, Faculty of Medicine, University of Helsinki, Haartmanninkatu 8, 00014 Helsinki, Finland
[c] Minerva Foundation Institute for Medical Research, Tukholmankatu 8, 00290 Helsinki, Finland
[d] Electron Microscopy Unit, Institute of Biotechnology, Helsinki Institute of Life Science, University of Helsinki, Viikinkaari 9c, 00014 Helsinki, Finland

ARTICLE INFO

Keywords:
ER subdomains
ER-mitochondria contact sites
SOAT1
Relative labeling index
Quantitative morphological analysis

ABSTRACT

The endoplasmic reticulum (ER) is a large, single-copy, membrane-bound organelle that comprises an elaborate 3D network of diverse structural subdomains, including highly curved tubules, flat sheets, and parts that form contacts with nearly every other organelle. The dynamic and complex organization of the ER poses a major challenge on understanding how its functioning – maintenance of the structure, distribution of its functions and communication with other organelles – is orchestrated. In this study, we resolved a unique localization profile within the ER network for several resident ER proteins representing a broad range of functions associated with the ER using immuno-electron microscopy and calculation of a relative labeling index (RLI). Our results demonstrated the effect of changing cellular environment on protein localization and highlighted the importance of correct protein expression level when analyzing its localization at subdomain resolution. We present new software tools for anonymization of images for blind analysis and for quantitative assessment of membrane contact sites (MCSs) from thin section transmission electron microscopy micrographs. The analysis of ER-mitochondria contacts suggested the presence of at least three different types of MCSs that responded differently to changes in cellular lipid loading status.

1. Introduction

The endoplasmic reticulum (ER) consists of an elaborate network of flat cisternae (aka sheets) and tubules that extends throughout the cell and occupies a large fraction of the cytoplasmic volume. The ER is classically divided into two interconnected compartments, rough ER (RER) and smooth ER (SER), depending on the presence or absence of ribosomes on the cytosolic face of the membrane (Baumann and Walz, 2001). Upon the identification of proteins that drive the formation of membrane domains of low or high curvature – sheets and tubules – a new view of the ER emerged, which is based on the structure itself rather than the appearance of ribosomes (Shibata et al., 2006). This view acknowledges the highly dynamic nature of ER structures, where sheets and tubules constantly transform into each other, and suggests that the curvature itself may dictate the partitioning of other proteins to create distinct functional domains (Puhka et al., 2012; Westrate et al., 2015).

The ER contributes to the production and folding of approximately one third of cellular proteins, has a key role in coordinating lipid metabolism, and constitutes a reservoir of calcium ions that act as signaling molecules to regulate essential cellular processes. The ER has a central role in organelle communication, as it forms membrane contacts with most other organelles such as mitochondria, endo/lysosomes, peroxisomes, lipid droplets (LDs), and plasma membrane (PM) (Wu et al., 2018). Peroxisome, LD, and autophagosome membrane contact sites (MCSs) have additional complexities because the biogenesis of these organelles begins in the ER as well. The dynamic and complex organization of the ER poses a major challenge on understanding how its functioning – maintenance of the structure, distribution of its functions and communication with other organelles – is orchestrated.

In this study, we characterized specific subdomain localizations of several resident ER proteins and ER-mitochondria contact sites during various lipid-loading states using transmission electron microscopy (TEM). We developed new software tools for anonymization of images for blind analysis and for quantitative assessment of membrane contact

* Corresponding author at: Institute of Biotechnology, Helsinki Institute of Life Science, University of Helsinki, Viikinkaari 9c, 00014 Helsinki, Finland.
E-mail address: Eija.Jokitalo@Helsinki.fi (E. Jokitalo).

https://doi.org/10.1016/j.ejcb.2021.151180
Received 7 July 2021; Received in revised form 23 September 2021; Accepted 28 September 2021
Available online 4 October 2021

sites from thin section TEM micrographs. We analyzed localization of five ER resident proteins, Sec61β, reticulon 4B (RTN4B), receptor expression-enhancing protein 5 (REEP5), seipin and sterol O-acyltransferase (SOAT1, aka acyl-CoA: cholesterol acyltransferase, ACAT1), representing a broad range of functions associated with the ER. Sec61β is an essential part of the polypeptide translocation channel (Greenfield and High, 1999); RTN4B and REEP5 are structural proteins involved in ER remodeling, membrane shaping and maintenance (Bjork et al., 2013; Voeltz et al., 2006); seipin regulates ER-LD contacts and cargo delivery (Salo et al., 2016); and SOAT1 is a cholesterol esterifying enzyme (Ikonen, 2008).

Using seipin as an example, we first showed the importance of correct protein expression level to its localization at subdomain resolution. We then resolved a unique localization profile within the ER network for each of the five proteins expressed at endogenous levels by calculating a relative labeling index (RLI) from immuno-EM images (Mayhew, 2011; Mayhew et al., 2002). The analysis of ER-mitochondria contacts suggested the presence of at least three different types of MCSs that responded differently to changes in cellular lipid loading status. Moreover, during lipid starvation, we observed relocalization of SOAT1 to the nuclear envelope (NE).

2. Materials and methods

2.1. Cell culture and treatments

Human epithelial carcinoma cells (A431) were cultured in DMEM (BioWhittaker, Lonza, Verviers, Belgium) containing 10% fetal bovine serum (Gibco, Invitrogen, Thermo Fisher Scientific, Waltham, MA), Ultra glutamine, penicillin and streptomycin (Lonza). For lipid starvation, cells were delipidated by culturing in serum-free medium supplemented with 5% lipoprotein-deficient serum for 3 days [LPDS was prepared as earlier described (Goldstein et al., 1983)]. When indicated, cells were loaded with cholesterol using the final concentration of 50 μM methyl-β-cyclodextrin (randomly methylated, Sigma C4555) complexes. DNA transfections and mild overexpression of seipin-sfGFP were done using Fugene HD (NGF; Promega, Madison, WI) according to manufacturer's instructions.

2.2. Antibodies

Antibody against GFP (ab290; abcam, Cambridge, the UK), RTN4B (AB-163; Kinasource Ltd, Dundee, UK), and REEP5 (sc-393508, Santa Cruz Biotechnology, Inc) were used as primary antibodies. When indicated, rabbit anti-sheep bridging antibody (313-001-003; Jackson ImmunoResearch Labs Inc., West Grove, PA) was used. Secondary anti-mouse and anti-rabbit antibodies were conjugated with 1.4 nm nanogold particles (Nanoprobes, Stony Brook, NY), or with Alexa 488 (A-11008; Life Technologies).

2.3. Generation of endogenously tagged seipin-sfGFP, SOAT1-sfGFP and sfGFP-Sec61B cell lines

Endogenously tagged seipin-sfGFP cell line as well as the seipin KO cell line overexpressing seipin-mEGFP were generated and validated as described (Salo et al., 2016). SOAT1-sfGFP and sfGFP-Sec61B cell lines were generated in a similar way. Briefly, to generate endogenously tagged SOAT1-sfGFP and sfGFP-Sec61β cell lines, CRISPR/Cas9 technology was used (Ran et al., 2013). Superfolder-GFP (Pedelacq et al., 2006) and a 3XGGGGS linker were inserted at the C-terminus of endogenous SOAT1 (validation below) or at the N-terminus of Sec61β (commonly used, in e.g. Addgene plasmids). A homology-directed repair template was generated by overlap PCR and transfected into A431 cells together with a vector encoding Cas9, sgRNA targeting the C-terminus of SOAT1 locus (target site, CGTTACGTGTTTTAGAA-GCT tgg) or N-terminus of Sec61β (target site, GGGCCGCCATACCATAT tgg) and a puromycin selection marker. Clones were isolated after transient selection with puromycin. Homozygously tagged cell lines were validated by genomic PCR and/or Western blot with an antibody against the endogenous protein (Mouse anti-SOAT1 (D-1), Santa Cruz sc-137013) or anti-GFP (Fig. S1).

2.4. Light microscopy

Cells were grown on coverslips and fixed with 4% formaldehyde (Electron Microscopy Sciences, Hatfield, PA) supplemented with 0.1 mM MgCl2, and 0.1 mM CaCl2 in phosphate-buffered saline (PBS), quenched with 50 mM NH4Cl, permeabilized with 0.1% Triton X-100, and then blocked with 0.2% bovine serum albumin (BSA) in Dulbecco PBS (Lonza). When appropriate, the cells were incubated consecutively with primary and secondary antibodies diluted in blocking solution. Samples were mounted in Mowiol (Hoechst, Frankfurt, Germany) supplemented with Dabco (Sigma-Aldrich). Wide-field images of fixed cells were taken with Zeiss AxioImager M2 482 epifluorescence micro-scope equipped with 63X/Plan-Apochromat/1.40 oil/M27 and 483 AxioCam HRm camera (Zeiss, Oberkochen, Germany) or with Leica DM6000B upright fluorescence wide field microscope equipped with 63X/1.25–0.75 HCX PL APO CS oil objective, Hamamatsu Or-ca-Flash 4.0 V2 sCMOS camera (Wetzlar, Germany). Images were acquired using Axio-Vision4 (Zeiss) or LAS X software (Leica).

2.5. Transmission electron microscopy

Cells grown on glass coverslips (thickness #1) were fixed with 2% glutaraldehyde in 0.1 M sodium cacodylate buffer, pH 7.4, for 30 min at RT, post-fixed with 1% reduced osmium tetroxide (OsO4) in same buffer, for 1 h on ice, dehydrated through series of ethanol and acetone, and flat embedded into Epon (TAAB 812) as described previously (Jokitalo et al., 2001). For immuno-EM, prior embedding as described above, cells were fixed with paraformaldehyde-lysine-periodate fixative for 2 h at RT (McLean and Nakane, 1974), permeabilized with 0.01% saponin, and immunolabelled sequentially with primary antibody and 1.4 nm nanogold-conjugated secondary antibody prior silver enhancement with HQ Silver kit (Nanoprobes, Stony Brook, NY). Silver precipitate was stabilized by incubations with 2% sodium acetate (NaOAc), 0.05% auric chloride (HAuCl4; 10 min on ice), and 0.3% sodium thiosulphate (Na2S2O3·5H2O).

65-nm thin sections were cut using Leica UCT6 microtome and post-stained with 0.5% uranyl acetate (SPI-Chem, USA) and 3% lead citrate (Leica Microsystems, Vienna, Aus-tria). TEM imaging was done with Jeol JEM-1400 (Jeol Ltd., Tokyo, Japan) operated at 80 kV, equipped with Gatan Orius SC 1000B bottom mounted CCD-camera (Gatan Inc., USA).

2.6. Quantitative analysis of TEM images

The distribution of the gold labeling was quantified as described (Mayhew, 2011; Mayhew et al., 2002), using Microscopy Image Browser (MIB; http://mib.helsinki.fi/) segmenting software (Belevich et al., 2016). 17 cells per condition were randomly selected at low magnification. Higher magnification images were acquired at 8000x at north and south positions relative to the nucleus in these randomly selected cells. Images were calibrated, contrast normalized and converted to 8-bit using MIB. For analysis, the images from different conditions were pooled together, shuffled, and anonymized using Rename and shuffle, and Restore tools of MIB (Fig. S2; In MIB: Menu →File → Rename and shuffle). Tutorials guiding for the use are available at http://mib.helsinki.fi/help/main2/ug_gui_menu_file_rename_and_shuffle.html. Segmentation of the cellular compartments was done in MIB. To assign the gold particles to the respective organelle, following categories of cellular compartments were defined as appropriate: ER sheet, ER tubule, nuclear envelope, ER-mitochondria contact site, ER-lipid droplet contact site,

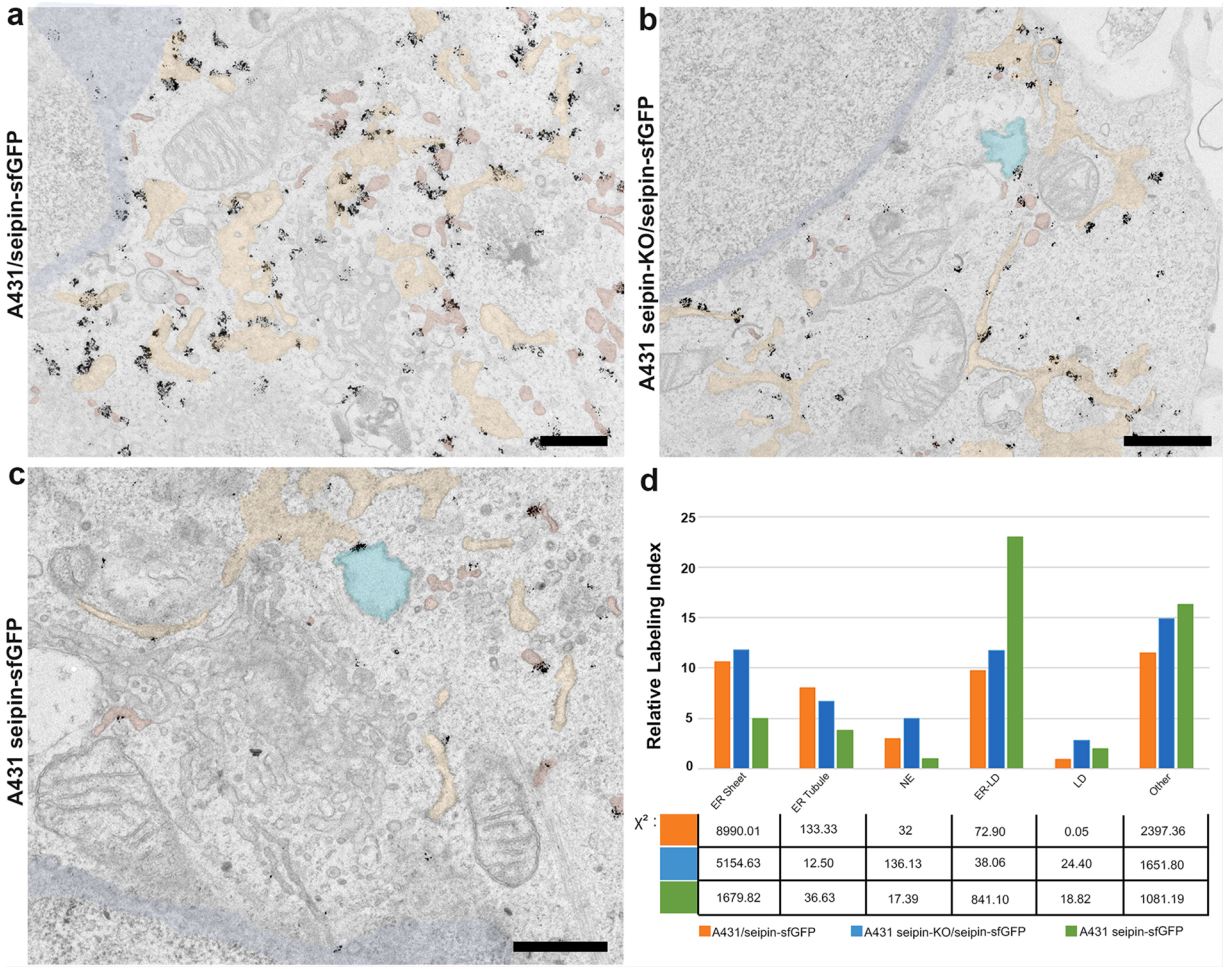

Fig. 1. Seipin localization in the ER depends on the expression level. TEM micrographs of A431 cells expressing seipin under three different expression levels: (a) transient overexpression, (b) stable retroviral overexpression on seipin knockout background and (c) endogenous protein tagging and expression. Cells were subjected to pre-embedding immunolabeling using anti-GFP antibody. (d) For quantitative analysis of the gold labeling, RLI was calculated based on the area of the respective cellular compartment and the attribution of the observed and expected number of the gold particles per organelle. Values under the plot show the compartmental chi-squared (χ^2) values. Total χ^2 values are 11625.7 for transient over-expression, 7017.5 for stable over-expression in seipin knockout background and 3675.0 for endogenously tagged cell line. The compartment is preferentially labelled, when RLI has a value > 1 and its χ^2 makes an important contribution to total χ^2. See also Fig. S2 for definition of cellular compartments and gold particle clusters and estimation of areas using point hit method. ER sheets are indicated with yellow, ER tubules with red, NE with blue and LD with cyan color. See Fig. S4 for original grayscale micrographs. Scale bars: 1 μm. (For interpretation of the references to colour in this figure legend, the reader is referred to the web version of this article.)

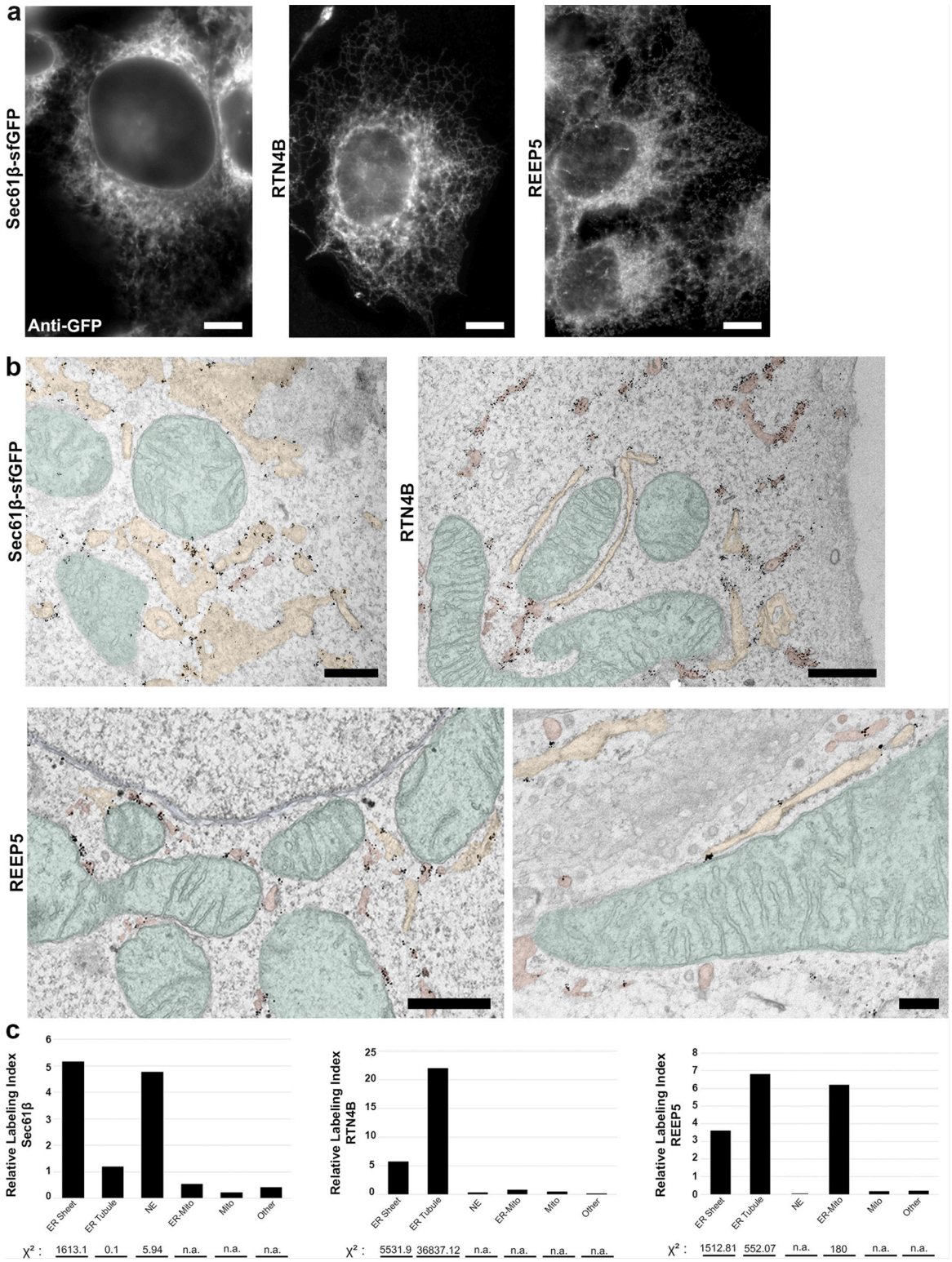

Fig. 2. Quantitative immuno-EM reveals individual localization profiles for resident ER proteins Sec61β, RTN4B, and REEP5. (a) Confocal light microscopy and (b) pre-embedding immunolabeling of A431 cells expressing endogenously tagged Sec61β-sfGFP, or endogenous RTN4B and REEP5. In RTN4B micrograph, black arrowhead indicates the presence of RTN4B in ER tubules, while black arrow shows the ER sheet devoid of labeling for RTN4B. In REEP5 micrograph, black arrowhead indicates the labeling of REEP5 at an ER-mitochondria contact site. (c) The preferred localization of each protein can be compared from the RLIs. Values under the plot show the compartmental chi-squared (χ^2) values. Total χ^2 values are 1941.9 for Sec61β, 44858.3 for RTN4B and 2801.1 for REEP5. The compartment is preferentially labelled, when RLI has a value > 1 and its χ^2 makes an important contribution to total χ^2. ER sheets are indicated with yellow, ER tubules with red, NE with blue and mitochondria with green color. See Fig. S4 for original grayscale micrographs. Scale bars: 10 μm in (a) and 500 nm in (b). (For interpretation of the references to colour in this figure legend, the reader is referred to the web version of this article.)

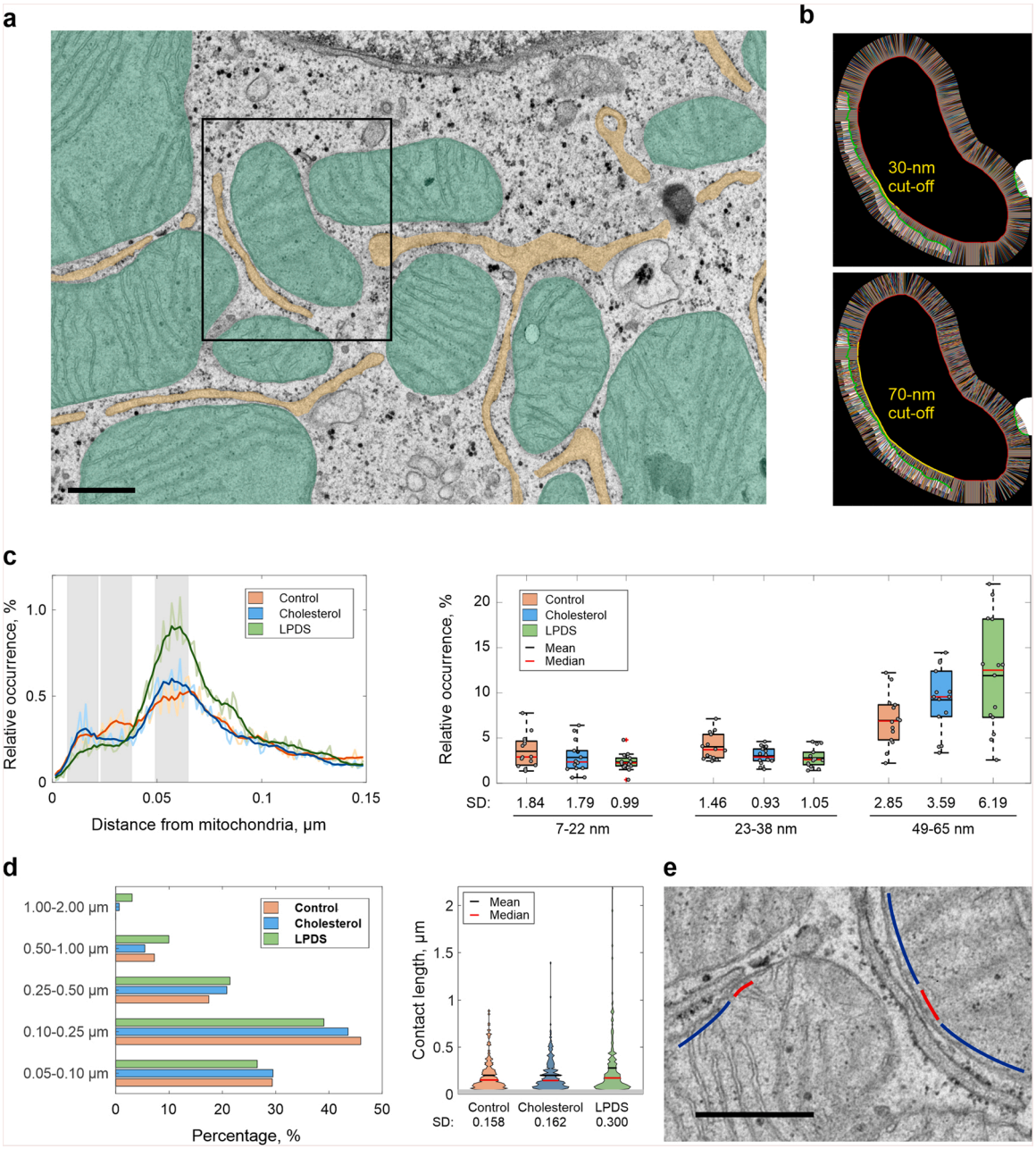

Fig. 3. ER-mitochondria contact site distribution changes pending on the lipid loading status. (a) TEM micrograph with segmented ER and mitochondria depicted in yellow and green, respectively. The rectangle box indicates the area magnified in the panel (b). (b) Examples of detected contacts using 30- (upper image) and 70-nm (lower image) cut-offs. The mitochondria and the ER are shown as red outline and white area, respectively. The colored lines represent the sampling rays originating from mitochondria's perimeter; the green points show positions where the generated rays hit the ER; the yellow points highlight the detected contact. (c) On left, averaged distribution of distances between ER and mitochondria in control (N = 93 mitochondrial profiles), cholesterol loading (N = 161), and lipid starvation (LPDS treatment; N = 146) conditions. Lighter lines are averaged data from all profiles, and darker lines are smoothened with the running averaged filter (window 7). On right, boxplots show the distribution of the average values per cell at 7–22, 23–38 and 49–65 nm distance groups. Values under the plot show the standard deviation (SD) for each group. (d) On left, relative distribution of contacts under 70 nm distance in 5 length categories in control, cholesterol loading, and lipid starvation. On right, violin plots show the distribution of lengths of these contacts. Values under the plot show the standard deviation (SD) for each condition. (e) Close-up view from (a) depicting tight ER-mitochondria contacts (red line) and wider ribosome-containing ER-mitochondria contacts (blue line). Scale bar: 500 nm. (For interpretation of the references to colour in this figure legend, the reader is referred to the web version of this article.)

mitochondria, lipid droplet, and others (Fig. S3a). Others category includes labeling on all other organelles not having own category and cytosolic labeling. ER sheet and tubule profiles were distinguished based on the presence or lack of membrane bound ribosomes, respectively (Puhka et al., 2007, 2012). To estimate the area of the cellular compartments, the Stereology tool of MIB (In MIB: Menu → Tools → Stereology) was used, where a grid with 230-nm spacing was placed on each image. Whenever a branch point fell on top of a cellular compartment, it was assigned to its respective category (Fig. S3c). Nuclear and extracellular area were excluded from calculations. Branch points per cellular compartment were calculated and the clusters of immuno-gold were annotated and assigned to corresponding cellular compartment (For the definition of immuno-gold clusters, see Fig. S2b). RLI was calculated based on the area of the respective cellular compartment and the attribution of the observed number (N_o) and expected number (N_e) of the gold particles per organelle (Mayhew, 2011; Mayhew et al., 2002). For

statistical analysis we used the chi-squared (χ^2) test (Sokal and Rohlf, 1981) using the formula $\chi^2 = (N_o\text{-}N_e)^2/N_e$. The compartment is preferentially labelled, when RLI has a value > 1 and its χ^2 makes an important contribution to total χ^2.

The numerical morphometric analysis of mitochondria-ER MCSs, 15 cells per condition were randomly selected at low magnification and then images at 5000 x at north and south positions relative to the nucleus were taken. Images were calibrated, contrast normalized and converted to 8-bit using MIB. Mitochondria and ER were segmented using MIB, and MCSs analyzed using a dedicated plug-in called MCcalc in MIB software platform (in MIB: Menu → Plug-ins → Organelle analysis → MCcalc) using probing distance 150 nm and accepting 5 pixel gaps. The rationale behind the MCcalc software is given in Appendix B and the graphical user interface and configuration features are described in Supplementary Data file. A video tutorial for the full workflow is available at http://mib.helsinki.fi/tutorials_tools.html → MCcalc plug-in.

3. Results

3.1. Protein overexpression results in the loss of specific ER subdomain localization

The concept of pre-embedding immuno-EM is that cells are mildly fixed by chemical crosslinking to preserve the morphology while maintaining the antigenicity; mildly permeabilized with glycosides (e.g. saponin) that perforate the membranes without dissolving them; immunolabelled with primary and nano-gold conjugated secondary antibodies; silver-enhanced to make nanoparticles visible prior to plastic embedding and preparation of thin sections for TEM analysis. Unfortunately, only a small fraction of primary antibodies work in immuno-EM, most likely because epitopes are either sensitive to fixatives or not accessible to antibodies when buried inside protein complexes or masked by lipids. Moreover, the process of generating specific primary antibodies for each protein of interest is time-consuming and nowadays often overcome by cloning of expression constructs where a tag is attached to the protein of interest and recognized by specific commercial antibodies. However, overexpressing the tagged version of a protein may cause misleading results.

To elaborate this, we analyzed the localization of seipin, which is a resident ER protein involved in lipid droplet (LD) formation (Salo et al., 2016), under three different expression levels: transient overexpression, stable retroviral overexpression on seipin knockout background and endogenous protein tagging and expression. The relative mRNA level under stable over-expression was four times higher compared to the wild type (Salo et al., 2016), whereas in transiently overexpressing cells the level is around 10–20 times higher. Interestingly, upon transient overexpression of seipin-sfGFP for 16 h, the protein was found to spread throughout the ER network (Fig. 1a). Similar results were obtained in seipin-KO cell line overexpressing seipin-GFP (Fig. 1b). However, in the

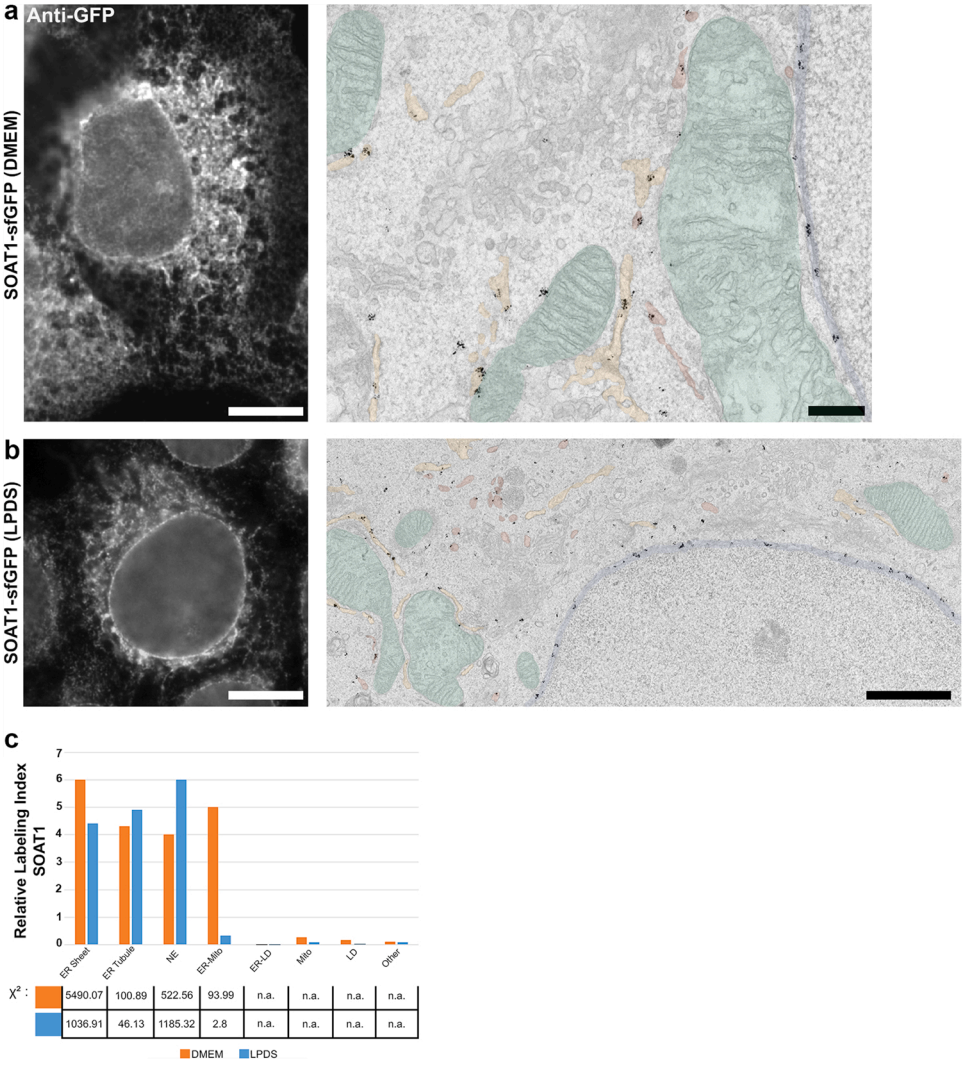

Fig. 4. Lipid starvation induces changes in the distribution of the cholesterol metabolic enzyme SOAT1 within the ER network. Confocal light microscopy and pre-embedding immunolabeling of A431 cells expressing endogenously tagged SOAT1-sfGFP (a) under normal growth conditions and (b) upon lipid starvation (LPDS treatment for 3 days). (c) The preferred localization under both conditions can be compared from the RLIs. Values under the plot show the compartmental chi-squared (χ^2) values. Total χ^2 values are 7351.4 for normal growth conditions (DMEM) and 2776.4 for lipid starvation (LPDS). The compartment is preferentially labelled, when RLI has a value > 1 and its χ^2 makes an important contribution to total χ^2. ER sheets are indicated with yellow, ER tubules with red, NE with blue and mitochondria with green color. See Fig. S4 for original grayscale micrographs. Scale bars: 10 μm in confocal images and 500 nm in TEM micrographs. (For interpretation of the references to colour in this figure legend, the reader is referred to the web version of this article.)

seipin-sfGFP stable cell line generated using CRISPR-Cas9 system to express seipin at the endogenous levels, we found a clear enrichment of seipin at ER-LD contact sites, which was not apparent in the two other samples (Fig. 1c). For quantitative analysis, we designed a new software tool that can be used to temporarily rename images, and then pool and shuffle images from different conditions for unbiased analysis (Fig. S2). Using this tool, the RLI was calculated for an anonymized pool of images. The results showed that in the endogenously sfGFP-tagged seipin cell line, seipin was enriched in ER-LD contact sites while in the overexpression systems, the protein was essentially evenly spread in the ER so that the specific subdomain localization at ER-LD contact sites was not evident (Fig. 1d). Thus, it is of utmost importance to maintain the protein at endogenous levels in cells when performing localization studies at organelle subdomain resolution.

3.2. Distinct distribution of ER resident proteins is resolved by electron microscopy

Light microscopy observations of Sec61β, RTN4B, and REEP5 revealed their general localization in the ER network of A431 cells (Fig. 2a). The distribution patterns of the proteins looked rather similar, making it difficult to conclude on their sub-organellar localization. Immuno-EM, on the other hand, allows analysis of protein localization in the context of surrounding organelles and organelle structure, e.g. on ER sheets, tubules, and specific organelle contact sites. Unlike light microscopy, immuno-EM and quantitative analysis of the gold labeling pinpointed unique localizations within the ER network for each protein investigated. Cells expressing endogenously tagged Sec61β-sfGFP showed exclusive localization of Sec61β on ER sheets and the NE, while immuno-EM against the endogenous RTN4B revealed clear preference for the curved regions of the ER: tubules and sheet edges. Immuno-EM against the endogenous REEP5 showed a preference over tubules and ER-mitochondria contact sites (Fig. 2b, c).

3.3. ER-mitochondria contact site distribution changes pending on lipid loading status

An important aspect of membrane contacts is that they do not lead to the fusion of membranes and mixing of luminal contents but allow crosstalk between adjacent membrane bilayers. Many tethering proteins have been identified and they can be used to analyze and manipulate the distribution, frequency and lifetime of the corresponding contacts (Paillusson et al., 2016). However, many native contacts await characterization and their typical width of a few tens of nanometers between juxtaposed membranes makes their morphological analysis at the EM level an attractive approach. Morphologically two types of ER-mitochondria contacts have been characterized. In the tight contacts, the two organelles are juxtaposed at a constant distance between 10 and 30 nm, and densities from specialized tethering complexes are typically seen (Csordas et al., 2006; Friedman et al., 2011; Wu et al., 2018). In the second type, mitochondria form contact with the ribosome-containing ER sheet, and the cleft between the membranes is wider, typically between 50 and 80 nm (Giacomello and Pellegrini, 2016). The number, length, and distance between the membranes in these contacts are regulated parameters of the cell; they contribute to define its biological function and provide the elements on which the cell can regulate the activity of this subcellular compartment (Giacomello and Pellegrini, 2016). For numerical morphometric analysis of organelle contacts, we developed a dedicated software to analyze them from TEM micrographs (Fig. 3a; plug-in called MCcalc in MIB software platform). MCcalc allows mapping of preferred distances between organelles, and more careful analysis of contacts within certain distance groups (Fig. 3b).

Here, we mapped the distribution of ER and mitochondria membrane distances under three different metabolic cues: normal culture conditions, lipid starvation (3 days cultivation in lipoprotein-deficient serum containing medium, LPDS) or after 30 min of acute cholesterol loading from a cyclodextrin complex (Chol). Our results point out several membrane distance areas, where changes occur upon changing the lipid loading status. Under normal growth condition, the number of contact sites peaked sharply at 15 and 30 nm, and more broadly around 60 nm distance between the ER and mitochondrial membranes, suggesting the presence of at least three different types of contact sites (Fig. 3c and e): two tight contact types between mitochondria and smooth ER membrane, and one wider contact type between mitochondria and ribosome-containing ER sheet. In the tight contact zone, ER membrane facing the mitochondria is ribosome-free, whereas ribosomes can be found from the opposing membrane of the sheet in this zone and on the mitochondria-facing membrane surrounding the tight contact zone (Fig. 3e). Upon cholesterol loading, contacts at 60 nm distance increased slightly while 30 nm ones were reduced. However, under lipid starvation (LPDS treatment), relatively fewer contact sites around 15–30 nm distances were observed and a clear increase in the number of 50–70 nm contacts occurred. Moreover, in LPDS, the contacts at distances under 70 nm were longer along the mitochondrial perimeter, as indicated by the increasing fraction of contacts above 250 nm, 500 nm or 1 μm in length (Fig. 3d).

3.4. Lipid loading status affects localization of endogenous cholesterol metabolic enzyme

To investigate if lipid starvation affects the subdomain localization of SOAT1 in the ER, we used immuno-EM and quantitative analysis of the gold labeling in cells expressing endogenously tagged SOAT1-sfGFP. Electron micrographs showed the distribution of the SOAT1 in the sheets, tubules, the NE, and ER-mitochondria contact sites (Fig. 4a). Under normal growth conditions, RLI revealed the highest preference of SOAT1 for sheets followed by ER-mitochondria contact sites, and slightly lower values in tubules and NE (Fig. 4c). However, the localization changed substantially once the cells were grown for 3 days in LPDS. This resulted in the accumulation of SOAT1 in the NE at the expense of ER sheets and ER-mitochondria contact sites (Fig. 4b, c).

4. Discussion

The dynamic nature of the ER includes transitions between ER sheets and tubules that can occur quite rapidly in response to changing cellular environment. We have shown that sheets are stabilized by ER-bound polyribosomes (Puhka et al., 2007) and that they form the persistent part of the ER network and mainly fluctuate at one locus without clear directionality (Joensuu et al., 2014). During cell division, protein translation and secretion halts, and concomitantly, the ER undergoes both spatial reorganization and structural transformation of sheets toward more fenestrated and tubular forms (Kumar et al., 2019; Puhka et al., 2007 and 2012). ER tubules are in direct connection to sheets and other tubules and form the dynamic part of the ER network.

The relative ratio of different ER structural domains (sheets, tubules and ER MCSs) is sensitive to changes in the ER proteome. We and others have reported that overexpression of ER structural proteins NOGO-A/RTN4A, RTN4B, FAM134C or the yeast reticulon orthologue Rtn1p generate long unbranched tubules, and overexpression of CLIMP63 leads to a dramatic proliferation of ER sheets (Kumar et al., 2021; Rämö et al., 2016; Shibata et al., 2010; Voeltz et al., 2006). Weak interactions between fluorescent protein tags engineered onto ER-resident proteins cytochrome b (5) and Sec61, or overexpression of calnexin induced the formation of organized smooth ER, OSER, by stabilizing ER sheets and expanding their amount (Korkhov and Zuber, 2009; Okiyoneda et al., 2004; Snapp et al., 2003). Overexpression of Xenopus or human Lamin B receptor in HeLa cells led to either NE invagination or large perinuclear aggregates of layered membrane stacks originating from the NE, depending on the expression level (Ellenberg et al., 1997; Ma et al., 2007).

Using seipin as an example, we show that overexpression of proteins

with low abundance might not induce morphological changes, but can lead to loss of its sub-organelle localization. At endogenous expression levels, seipin is enriched in ER-LD contact sites where it performs its function (Salo et al., 2019), while when overexpressed, the protein spreads evenly across ER sheets and tubules. Therefore, it is important to bear in mind that protein localization should be determined at endogenous protein levels. Moreover, when characterizing a novel ER protein, we recommend against studying their sub-organelle localization by co-expressing Reticulons and CLIMP63 as ER tubule and sheet markers, as their expression easily induces changes to the normal sheet-tubule organization. In our mind, expression of soluble luminal marker proteins with C-terminal KDEL to study the ER is the safest option, as in case of the overload, the marker protein saturates the ER retention system and can be detected in the cis-Golgi.

Here, we characterized specific subdomain localization of several resident ER proteins and demonstrated the effect of changing cellular environment on protein localization using immuno-EM and calculation of RLI. Had we used the tripartite classification of sheets, tubules and NE, we would not have been able to show clear differences in subdomain localization for each protein. However, immuno-EM allows determination of localization not only with respect to organelle structure but also to the surrounding environment. When organelle contact sites were included as separate categories, we were able to reveal individual localization profiles for the proteins.

Quantification of immunolabeling on TEM images usually involves estimating the labeling density (LD), i.e. relative number of gold particles falling on different compartments. The main disadvantage of this approach is that the observed labeling frequencies are biased against more voluminous or extensive compartments, as they appear more frequently in the micrographs. This means that even if two compartments contain the same concentration of the same antigen, more labeling is counted on the larger compartment. Therefore, estimation of RLI offers a reliable way for quantification as RLI is irrespective of the size or the amount of target object (Mayhew et al., 2002). This is especially critical when determining the subdomain localization within the ER, where the abundance of various structures in different categories is different and changes upon altering conditions. The basis of RLI is to compare the expected distribution in case of random (non-specific) labeling with the actual observed distribution of gold particles. Here we showed that lipid starvation induced both dramatic changes in the amount and distribution of ER-mitochondria contacts and to the sub-organelle relocalization of the cholesterol metabolic enzyme SOAT1 from ER-mitochondria contact sites to the NE. As RLI is irrespective of the occurrence of the contact sites, the loss of SOAT1 labeling in ER-mitochondria contacts cannot be explained by a technical fault. What this intriguing SOAT1 localization and its changes upon altering lipid loading status biologically signifies, awaits further studies.

ER-mitochondria contacts comprise functionally specialized compartments whose activity and regulation is directed by the width of the cleft that separates the cytosolic faces of these organelles (Wang et al., 2015). Thin sectioning allows organelles and their contact sites to be visualized under the TEM at optimal lateral resolution. However, ultrathin sections represent an extremely small fraction of the total specimen and, consequently, very limited number of contacts are visualized. To compensate this, random sampling is a prerequisite, as it will give every part of the specimen exactly the same chance of being selected. We developed dedicated software tools for qualitative and quantitative analysis of membrane contracts from thin-section TEM images. MCcalc software enables simultaneous analysis of multiple parameters such as surface of the organelles of interest, extent of the contact, intermembrane distance at the contact as well as their occurrence and changes in the extent. Furthermore, Rename and shuffle, and Restore software tools enable anonymization of images for segmentation and analysis. Here, we mapped the distribution of ER and mitochondria membrane distances under three different metabolic cues, and showed that under lipid starvation the tight contacts around 15 and 30 nm distance decrease and wider ribosome-containing ER-mitochondria contacts increase in occurrence and in length. The tight ribosome-free ER and wider ribosome-containing ER –mitochondria contacts are often found to be in continuity with each other (see Fig. 3a and e). The tight ER-mitochondria contacts have a role in maintaining lipid and Ca2+ homeostasis and have been implicated in the etiology of metabolic and degenerative disorders (Giorgi et al., 2015; Naon and Scorrano, 2014; Raturi and Simmen, 2013; Rieusset, 2017; Vance, 2014; Vallese et al., 2020). The local Ca2+ coupling can be weakened and strengthened by destruction and enforcement of the inter-organellar protein linkage, respectively (Csordas et al., 2006). ER stress doubles the number of tight ER-mitochondria contacts and increases the Ca2+ flux, leading to higher oxygen con-sumption within mitochondria (Bravo et al., 2011; Csordas et al., 2006). Glycoprotein 78 E3 ubiquitin ligase protein, an ER membrane-anchored ubiquitin ligase (E3), has been implicated in the formation of the ribosome-containing ER-mitochondria contacts, but much less is known about the function of these wider contacts (Wang et al., 2015). Recently ribosome-containing ER-mitochondria contacts were implicated for very-low-density lipoprotein (VLDL) secretion from the liver, thereby connecting intracellular and systemic control mechanisms for lipid metabolism and homeostasis (Anastasia et al., 2021). However, much remains unknown about these structures and their correlation to specific functions.

In conclusion, quantitative immuno-EM and thin section TEM provide attractive tools for characterization of specific subdomain localizations of resident ER proteins and ER-organelle contact sites. Our results suggest that functional subdomain distribution extends beyond classical sheet, tubule and nuclear envelope sub-compartment division, and that organelle contact sites play important role in defining functional subdomains within the ER network. As the ER network is highly dynamic, ultimately we will need correlative light and EM techniques combining ultrafast sub-diffraction limited live cell imaging of proteins expressed at endogenous levels with the resolving power of the EM to give better insights into functional ER subdomains.

Funding

This work was supported by the Academy of Finland, Finland (project no. 1287975 and 1331998 to E.J., 324929 to E.I.); the Sigrid Jusélius Foundation, Finland (E.J., E.I.); the Biocenter Finland, Finland (E.J., and I.B.); the Helsinki Institute of Life Science Fellow's program, Finland (E.J., E.I.); Foundation Leducq, USA (E.I.); and Jane and Aatos Erkko Foundation, Finland (E.I.).

CRediT authorship contribution statement

Behnam Lak: Investigation, Methodology, Formal analysis, Writing – original draft preparation, Visualization. **Shiqian Li**: Methodology, Resources. **Ilya Belevich**: Software, Visualization. **Sreesha Sree**: Writing – original draft preparation. **Rebeka Butkovic**: Formal analysis. **Elina Ikonen**: Conceptualization, Resources, Supervision, Funding acquisition, Writing – review & editing. **Eija Jokitalo**: Conceptualization, Supervision, Funding acquisition, Writing – review & editing, Project management. All authors have read and agreed to the published version of the manuscript.

Declaration of Competing Interest

The authors report no declarations of interest.

Acknowledgements

We thank Electron Microscopy Unit (EMBI) and Light Microscopy Unit of the Institute of Bio-technology, University of Helsinki for excellent support during this project. B.L. was a graduate student in the Doctoral Programme in Integrative Life Science, University of Helsinki.

Appendix A. Supporting information

Supplementary data associated with this article can be found in the online version at doi:10.1016/j.ejcb.2021.151180.

References

Anastasia, I., Ilacqua, N., Raimondi, A., Lemieux, P., Ghandehari-Alavijeh, R., Faure, G., Mekhedov, S.L., Williams, K.J., Caicci, F., Valle, G., Giacomello, M., Quiroga, A.D., Lehner, R., Miksis, M.J., Toth, K., Vallim, T.Q.D., Koonin, E.V., Scorrano, L., Pellegrini, L., 2021. Mitochondria-rough-ER contacts in the liver regulate systemic lipid homeostasis. Cell Rep. 34, 108873.

Baumann, O., Walz, B., 2001. Endoplasmic reticulum of animal cells and its organization into structural and functional domains. Int. Rev. Cytol. 205, 149–214.

Belevich, I., Joensuu, M., Kumar, D., Vihinen, H., Jokitalo, E., 2016. Microscopy Image Browser: a platform for segmentation and analysis of multidimensional datasets. PLoS Biol. 14, 1002340.

Bjork, S., Hurt, C.M., Ho, V.K., Angelotti, T., 2013. REEPs are membrane shaping adapter proteins that modulate specific G Protein-coupled receptor trafficking by affecting ER Cargo capacity. PLoS One 8, 76366.

Bravo, R., Vicencio, J.M., Parra, V., Troncoso, R., Munoz, J.P., Bui, M., Quiroga, C., Rodriguez, A.E., Verdejo, H.E., Ferreira, J., Iglewski, M., Chiong, M., Simmen, T., Zorzano, A., Hill, J.A., Rothermel, B.A., Szabadkai, G., Lavandero, S., 2011. Increased ER-mitochondrial coupling promotes mitochondrial respiration and bioenergetics during early phases of ER stress. J. Cell Sci. 124, 2143–2152.

Csordas, G., Renken, C., Varnai, P., Walter, L., Weaver, D., Buttle, K.F., Balla, T., Mannella, C.A., Hajnoczky, G., 2006. Structural and functional features and significance of the physical linkage between ER and mitochondria. J. Cell Biol. 174, 915–921.

Ellenberg, J., Siggia, E.D., Moreira, J.E., Smith, C.L., Presley, J.F., Worman, H.J., Lippincott-Schwartz, J., 1997. Nuclear membrane dynamics and reassembly in living cells: targeting of an inner nuclear membrane protein in interphase and mitosis. J. Cell Biol. 138, 1193–1206.

Friedman, J.R., Lackner, L.L., West, M., DiBenedetto, J.R., Nunnari, J., Voeltz, G.K., 2011. ER tubules mark sites of mitochondrial division. Science 334, 358–362.

Giacomello, M., Pellegrini, L., 2016. The coming of age of the mitochondria-ER contact: a matter of thickness. Cell Death Differ. 23, 1417–1427.

Giorgi, C., Missiroli, S., Patergnani, S., Duszynski, J., Wieckowski, M.R., Pinton, P., 2015. Mitochondria-associated membranes: composition, molecular mechanisms, and physiopathological implications. Antioxid. Redox Signal. 22, 995–1019.

Goldstein, J.L., Basu, S.K., Brown, M.S., 1983. Receptor-mediated endocytosis of low-density lipoprotein in cultured cells. Methods Enzymol. 98, 241–260.

Greenfield, J.J.A., High, S., 1999. The Sec61 complex is located in both the ER and the ER-Golgi intermediate compartment. J. Cell Sci. 112, 1477–1486.

Ikonen, E., 2008. Cellular cholesterol trafficking and compartmentalization. Nat. Rev. Mol. Cell Biol. 9, 125–138.

Joensuu, M., Belevich, I., Rämö, O., Nevzorov, I., Vihinen, H., Puhka, M., Witkos, T.M., Lowe, M., Vartiainen, M.K., Jokitalo, E., 2014. ER sheet persistence is coupled to myosin 1c-regulated dynamic actin filament arrays. Mol. Biol. Cell 25, 1111–1126.

Jokitalo, E., Cabrera-Poch, N., Warren, G., Shima, D.T., 2001. Golgi clusters and vesicles mediate mitotic inheritance independently of the endoplasmic reticulum. J. Cell Biol. 154, 317–330.

Korkhov, V.M., Zuber, B., 2009. Direct observation of molecular arrays in the organized smooth endoplasmic reticulum. BMC Cell Biol. 10, 59.

Kumar, D., Golchoubian, B., Belevich, I., Jokitalo, E., Schlaitz, A.-L., 2019. REEP3 and REEP4 determine the tubular morphology of the endoplasmic reticulum during mitosis. Mol. Biol. Cell 30, 1377–1389.

Kumar, D., Lak, B., Suntio, T., Vihinen, H., Belevich, I., Viita, T., Xiaonan, L., Vartiainen, A., Vartiainen, M., Varjosalo, M., Jokitalo, E., 2021. RTN4B interacting protein FAM134C promotes ER membrane curvature and has a functional role in autophagy. Mol. Biol. Cell 32, 1158–1170.

Ma, Y., Cai, S., Lv, Q.L., Jiang, Q., Zhang, Q., Sodmergen, Zhai, Z.H., Zhang, C.M., 2007. Lamin B receptor plays a role in stimulating nuclear envelope production and targeting membrane vesicles to chromatin during nuclear envelope assembly through direct interaction with importin beta. J. Cell Sci. 120, 520–530.

Mayhew, T.M., 2011. Mapping the distributions and quantifying the labelling intensities of cell compartments by immunoelectron microscopy: progress towards a coherent set of methods. J. Anat. 219, 647–660.

Mayhew, T.M., Lucocq, J.M., Griffiths, G., 2002. Relative labelling index a novel stereological approach to test for non-random immunogold labelling of organelles and membranes on transmission electron microscopy thin sections. J. Microsc. 205, 153–164.

McLean, I.W., Nakane, P.K., 1974. Periodate-Lysine-Paraformaldehyde fixative - new fixative for immunoelectron microscopy. J. Histochem. Cytochem. 22, 1077–1083.

Naon, D., Scorrano, L., 2014. At the right distance: ER-mitochondria juxtaposition in cell life and death. Biochim. Biophys. Acta 1843, 2184–2194.

Okiyoneda, T., Harada, K., Takeya, M., Yamahira, K., Wada, I., Shuto, T., Suico, M.A., Hashimoto, Y., Kai, H., 2004. Delta F508 CFTR pool in the endoplasmic reticulum is increased by calnexin overexpression. Mol. Biol. Cell 15, 563–574.

Paillusson, S., Stoica, R., Gomez-Suaga, P., Lau, D.H.W., Mueller, S., Miller, T., Miller, C. C.J., 2016. There's something wrong with my MAM, the ER-mitochondria axis and neurodegenerative diseases. Trends Neurosci. 39, 146–157.

Pedelacq, J.D., Cabantous, S., Tran, T., Terwilliger, T.C., Waldo, G.S., 2006. Engineering and characterization of a superfolder green fluorescent protein. Nat. Biotechnol. 24, 79–88.

Puhka, M., Joensuu, M., Vihinen, H., Belevich, I., Jokitalo, E., 2012. Progressive sheet-to-tubule transformation is a general mechanism for endoplasmic reticulum partitioning in dividing mammalian cells. Mol. Biol. Cell 23, 2424–2432.

Puhka, M., Vihinen, H., Joensuu, M., Jokitalo, E., 2007. Endoplasmic reticulum remains continuous and undergoes sheet-to-tubule transformation during cell division in mammalian cells. J. Cell Biol. 179, 895–909.

Ran, F.A., Hsu, P.D., Wright, J., Agarwala, V., Scott, D.A., Zhang, F., 2013. Genome engineering using the CRISPR-Cas9 system. Nat. Protoc. 8, 2281–2308.

Raturi, A., Simmen, T., 2013. Where the endoplasmic reticulum and the mitochondrion tie the knot: The mitochondria-associated membrane (MAM). Biochim. Biophys. Acta. 1833, 213–224.

Rieusset, J., 2017. Role of endoplasmic reticulum-mitochondria communication in type 2 diabetes. Adv. Exp. Med. Biol. 997, 171–186.

Rämö, O., Kumar, D., Gucciardo, E., Joensuu, M., Saarekas, M., Vihinen, H., Belevich, I., Smolander, O.P., Qian, K., Auvinen, P., Jokitalo, E., 2016. NOGO-A/RTN4A and NOGO-B/RTN4B are simultaneously expressed in epithelial, fibroblast and neuronal cells and maintain ER morphology. Sci. Rep. 6, 35969.

Salo, V.T., Belevich, I., Li, S., Karhinen, L., Vihinen, H., Vigouroux, C., Magre, J., Thiele, C., Hölttä-Vuori, M., Jokitalo, E., Ikonen, E., 2016. Seipin regulates ER-lipid droplet contacts and cargo delivery. EMBO J. 35, 2699–2716.

Salo, V.T., Li, S., Vihinen, H., Hölttä-Vuori, M., Szkalisity, A., Horvath, P., Belevich, I., Peränen, J., Thiele, C., Somerharju, P., Zhao, H., Santinho, A., Thiam, A.R., Jokitalo, E., Ikonen, E., 2019. Seipin facilitates triglyceride flow to lipid droplet and counteracts droplet ripening via endoplasmic reticulum contact. Dev. Cell 50, 478–493 e9.

Shibata, Y., Shemesh, T., Prinz, W.A., Palazzo, A.F., Kozlov, M.M., Rapoport, T.A., 2010. Mechanisms determining the morphology of the peripheral ER. Cell 143, 774–788.

Shibata, Y., Voeltz, G.K., Rapoport, T.A., 2006. Rough sheets and smooth tubules. Cell 126, 435–439.

Snapp, E.L., Hegde, R.S., Francolini, M., Lombardo, F., Colombo, S., Pedrazzini, E., Borgese, N., Lippincott-Schwartz, J., 2003. Formation of stacked ER cisternae by low affinity protein interactions. J. Cell Biol. 163, 257–269.

Sokal, R.R., Rohlf, F.J., 1981. Biometry. In: The Principles and Practice of Statistics in Biological Research, 2nd ed. W. H. Freeman, San Francisco, pp. 154–155.

Vallese, F., Barazzuol, L., Maso, L., Brini, M., Cali, T., 2020. ER-mitochondria calcium transfer, organelle contacts and neurodegenerative diseases. In: Islam, M.S. (Ed.), Calcium Signaling, Advances in Experimental Medicine and Biology 1131, 2nd ed., 2020. Springer Nature, Switzerland, pp. 719–746.

Vance, J.E., 2014. MAM (mitochondria-associated membranes) in mammalian cells: lipids and beyond. Biochim. Biophys. Acta. 1841, 595–609.

Voeltz, G.K., Prinz, W.A., Shibata, Y., Rist, J.M., Rapoport, T.A., 2006. A class of membrane proteins shaping the tubular endoplasmic reticulum. Cell 124, 573–586.

Wang, P.T.C., Garcin, P.O., Fu, M., Masoud,i, M., St-Pierre, P., Pante, N., Nabi, I.R., 2015. Distinct mechanisms controlling rough and smooth endoplasmic reticulum contacts with mitochondria. J. Cell Sci. 128, 2759–2765.

Westrate, L.M., Lee, J.E., Prinz, W.A., Voeltz, G.K., 2015. Form follows function: the importance of endoplasmic reticulum shape. Annu. Rev. Biochem. 84, 791–811.

Wu, H.X., Carvalho, P., Voeltz, G.K., 2018. Here, there, and everywhere: the importance of ER membrane contact sites. Science 361, eaan5835.